High-spin states and neutron-hole influence in ^{209}At†

T. P. Sjoreen, G. Schatz,* S. K. Bhattacherjee,‡ B. A. Brown,§ D. B. Fossan, and P. M. S. Lesser¶
Department of Physics, State University of New York, Stony Brook, New York 11794
(Received 6 April 1976)

The properties of high-spin states in ^{209}At have been studied with the ^{206}Pb(^{6}Li, $3n\gamma$)^{209}At reaction. In-beam measurements with Ge(Li) detectors of γ-ray excitation functions, γ-γ coincidences, γ-ray angular distributions, and pulsed beam-γ timing were made to establish decay schemes, level energies, spin-parity assignments, isomeric lifetimes, and magnetic moments. High-spin states involving three valence protons in the $1h_{9/2}$, $2f_{7/2}$, or $1i_{13/2}$ orbitals were identified. The electromagnetic properties observed in ^{209}At were compared with those in the closed-neutron core nucleus ^{211}At to examine the influence of the two neutron holes on the proton structure; microscopic calculations of this influence were carried out in perturbation theory.

[NUCLEAR REACTIONS ^{206}Pb(^{6}Li, $3n\gamma$), E_{Li} = 29–34 MeV; measured γ-excitations, γ-γ coincidences, γ-$W(\theta)$, pulsed beam-γ timing, perturbed angular distributions; deduced level scheme, γ multipolarities, J^{π}, $T_{1/2}$, $B(E2)$, g factor; perturbation calculations.]

I. INTRODUCTION

Considerable success has been achieved in the understanding of the structure of nuclei near the doubly closed ^{208}Pb core nucleus ($Z = 82, N = 126$) in terms of the shell model. Effective operators for the nuclear and electromagnetic interactions can be extracted for valence nucleons from a comparison of theoretical calculations and experimental information. Calculations of the shell-model structure for valence protons of the $N = 126$ nuclei and for valence neutrons of the $Z = 82$ nuclei are fairly complete.[1,2] For nuclei that contain both valence protons and neutrons, however, the shell-model space becomes considerably larger making complete calculations essentially impossible. Recent studies[3,4] of $N = 124$ nuclei have been aimed at understanding the influence of the two neutron holes $(\nu)^{-2}$ of the ^{206}Pb core on the valence proton structure as observed in $N = 126$ nuclei. Different theoretical approaches taken to explain the experimental data for these $N = 124$ nuclei, especially for the proton-hole nucleus ^{205}Tl,[5] have probed these effects; a lack of experimental data for the $N = 124$ proton-particle nuclei including ^{209}At has prevented similar studies for these cases. Recently, the core-particle coupling model has been used to describe ^{209}At.[4] The high-spin $(\pi)^3$ states occurring in ^{211}At are well understood in terms of $(h_{9/2})^3$, $(h_{9/2})^2 f_{7/2}$, and $(h_{9/2})^2 i_{13/2}$ protons coupled to the ^{208}Pb core.[6,7] The purpose of the present study is to obtain experimentally the properties of the high-spin states in ^{209}At and to compare these results with theoretical calculations in order to evaluate the influence of the $(\nu)^{-2}$ states of the ^{206}Pb core.

At the beginning of the present study, the only available information on ^{209}At involved low-spin states which were populated by β decay of ^{209}Rn.[8] To investigate the high-spin states of ^{209}At, in-beam γ-ray measurements via the ^{206}Pb(^{6}Li, $3n$) fusion-evaporation reaction[9] were made. This $\Delta Z = 3$ reaction gave the appropriate high-spin selectivity in the ^{209}At nucleus.[10] The level scheme and electromagnetic properties, namely, transition probabilities and moments, were determined. Preliminary results of these measurement have been reported previously.[11] An independent study employing the ^{209}Bi(α, $4n$) reaction has also recently been performed to investigate high-spin states in ^{209}At.[12]

In the present work, the theoretical interpretations of the ^{209}At data include a microscopic calculation in which the influence of the neutron-hole configurations on the electromagnetic properties are calculated in perturbation theory; comparisons between the $N = 126$ and $N = 124$ nuclei are made. This approach is complimentary to the core-particle coupling calculation by Paar[4] and to the interpretation by Bergström *et al.*[12] of the energy shifts between the $N = 126$ and $N = 124$ high-spin levels in terms of a P_2 force.

II. EXPERIMENTAL METHODS AND PROCEDURE

The ^{206}Pb(^{6}Li, $3n$)^{209}At reaction was used to populate high-spin states in ^{209}At. Previous studies had demonstrated that considerable experimental information about the nuclear level structure and the electromagnetic properties can be learned from γ-decay studies following (^{6}Li, xn) reactions.[10] The (HI, xn) fusion-evaporation reactions have

several features which are very useful to γ-ray spectroscopy[9]: (1) the strong dependence of the cross section for x evaporated neutrons on the beam energy means that a specific residual nucleus can be populated, nearly uniquely, by choosing the proper beam energy; (2) the large amount of orbital angular momentum brought in perpendicular to the beam axis leads to the formation of high-spin states that are highly aligned in low-m substates; and (3) the subsequent γ-ray decay proceeds through yrast levels via stretched transitions, $J \rightarrow J-L$, where L refers to the γ-ray multipolarity. Several γ-ray measurements are required in conjunction with these reaction features to obtain the desired experimental information. For the present ^{209}At study, γ-excitation, γ-γ coincidence, γ angular distribution, pulsed beam-γ timing, and perturbed angular distribution measurements were made.

The γ-excitation study was performed in order to help in the identification of γ rays originating from the nucleus of interest. The energy dependence of the γ-ray yields for a specific residual nucleus are similar.[9] In addition, the excitation measurements allow the selection of the bombarding energy for optimum relative yield. A level scheme for the residual nucleus ^{209}At was constructed on the basis of the γ-γ coincidence results and the relative yields obtained from the angular distribution measurements. Strong J^{π} assignments and γ-ray multipolarities were obtained from the angular distributions with the assumptions that the states are aligned in low-m substates and that the dominant γ decay proceeds via yrast levels by stretched transitions.[9] Lifetime and conversion coefficient information aid in these assignments. The weaker γ rays may involve non-yrast levels and because of structure reasons, may also represent nonstretched transitions. Time differential pulsed beam-γ measurements were made to identify delayed transitions and to obtain lifetime results for isomeric states. The perturbed angular distribution measurements were performed with an external magnetic field and the pulsed beam to determine magnetic moments of the isomers.

The in-beam γ-ray measurements were carried out with ^{6}Li ions from the Stony Brook tandem Van de Graaff accelerator. The targets were enriched (99%) metallic foils of ^{206}Pb, 10 to 18 mg/cm^2 thick. For the g-factor measurements, a similar target 68 mg/cm^2 thick was used in order to stop the beam. In these experiments, several Ge(Li) detectors with efficiencies of ~12% for 1.33-MeV γ rays were used. These detectors typically had in-beam resolutions of 2–3 keV at 1.33 MeV. In addition, for γ rays with energies less than 150 keV, a 5-mm planar intrinsic Ge detector was employed; this detector had a resolution of 0.5 keV at 122 keV.

A. γ excitation function

The γ-ray excitation measurements were made with a Ge(Li) detector positioned at 90° to the beam. The beam energy was varied from 29 to 34 MeV in increments of 1 MeV, and at each energy, a singles γ-ray spectrum was accumulated. Normalization was achieved by current integration. The yield for a given γ ray was determined by fitting the photopeak to a Gaussian distribution along with either a linear or quadratic background. After correcting for the detector efficiency, the relative intensities of the γ rays at 90° as a function of energy were obtained. Most of the subsequent experiments were carried out at a ^{6}Li beam energy of 34 MeV which yielded the highest (^{6}Li, $3n$) cross section in this energy range.

B. Angular distributions

The γ-ray angular distribution measurements were made with a movable Ge(Li) detector positioned 10 cm from the target, while another Ge(Li) detector placed at 90° to the beam served as a monitor. γ-ray singles spectra were accumulated at 90°, 120°, 135°, 150°, and 153° for a beam energy of 34 MeV. After obtaining the photopeak area, the data were normalized; this included dead-time corrections obtained from a current regulated pulser and corrections for geometric effects. A function of the form $W(\theta) = I_{\gamma}[1 + A_2 P_2(\cos\theta) + A_4 P_4(\cos\theta)]$ was fitted to the resulting angular distribution data to obtain the intensity I_{γ} and the values of the Legendre polynomial coefficients A_2 and A_4.

C. γ-γ coincidence

To perform the γ-γ coincidence measurements, two Ge(Li) detectors were each positioned at about 100° with respect to the beam axis and about 160° relative to each other to reduce the coincidence rate due to 511-keV annihilation radiation. A standard fast-slow coincidence system was employed and the data were stored on magnetic tape event by event. The analysis of the data was carried out off-line by scanning the data to obtain coincidence spectra for various digital γ-ray gates of interest. Appropriate Compton background gates were also made for each γ ray and subtracted out; random events were negligible.

To observe coincidences with γ rays of energies less than 150 keV, a γ-γ coincidence measurement with one Ge(Li) detector and the planar intrinsic-Ge detector was also carried out.

D. Pulsed beam-γ timing

For the pulsed beam timing measurements, the ^{6}Li beam was pulsed at repetition rates of both 1

and 4 μsec, with a pulse width of about 3 nsec full width at half maximum (FWHM), and the Ge(Li) detector was positioned at 90° to the beam. Delayed γ-ray spectra were collected on line for several time windows from 10 nsec to 4 μsec. With these data it was possible to obtain lifetime information simultaneously from all γ rays belonging to the decay modes of isomeric states. Delayed spectra were also accumulated with the intrinsic Ge detector.

Time differential measurements for specific delayed γ rays were also made to obtain more accurate lifetime results. These measurements were performed by pulsing the beam and collecting time spectra from a time-to-amplitude converter (TAC) for the γ rays of interest. Also, TAC spectra were collected for appropriate Compton regions. To extract lifetimes, the Compton TAC spectra were subtracted from the photopeak TAC spectra, and the resulting data were fitted to the function $Ae^{-t/\tau}+B$ where B is a constant background, A the amplitude at $t=0$, and τ the mean lifetime. When needed, a two-lifetime function was used in the data fits.

E. Perturbed angular distributions

The g-factor measurements were made by a pulsed beam experiment utilizing the time differential perturbed angular distribution (TDPAD) method.[13] An external magnetic field of $H=12.3\pm0.1$ kG was applied perpendicular to the detector plane. With Ge(Li) detectors placed at $+45°$ and $-45°$ with respect to the beam axis, the intensity modulations as a function of time due to the Larmor precession of the magnetic moment have opposite phases. Thus, the timing data were evaluated using the standard expression $R(t)=[N(45°,t)-N(-45°,t)]/[N(45°,t)+N(-45°,t)]$, where $N(\theta,t)$ denotes the yield after background subtraction. If the A_4 term is small, $R(t)$ reduces to $R(t)=[3A_2/(4+A_2)]\times\sin[2(\omega_L t-\Delta\theta)]$, where $\omega_L=g\mu_N H/\hbar$ is the nuclear Larmor precession. The phase $\Delta\theta$ accounts for any deviation from the symmetric detector

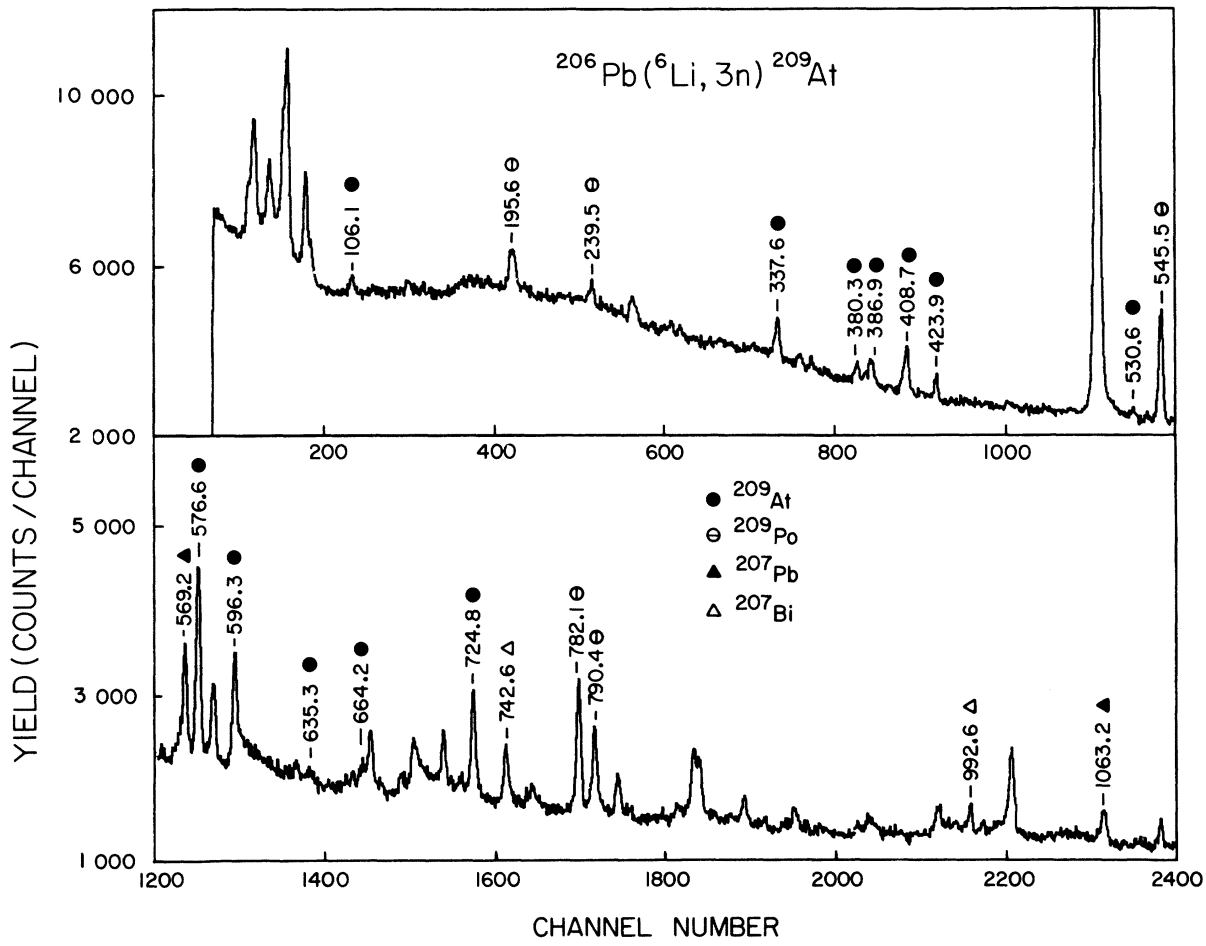

FIG. 1. The γ-ray spectrum observed in a Ge(Li) spectrometer at 90° to the beam for the bombardment of a thick ^{206}Pb target with 34-MeV ^{6}Li ions.

TABLE I. Reaction channels for $^{6}Li + ^{206}Pb$ based on ground-state γ-ray transitions.

Reaction channel	Relative intensity at 34 MeV
$(^{6}Li, 3n)^{209}At$	10
$(^{6}Li, 2n)^{210}At$	< 1
$(^{6}Li, pn)^{210}Po$	< 1
$(^{6}Li, \alpha n)^{207}Bi$	4
$(^{6}Li, \alpha p)^{207}Pb$	3
$(^{6}Li, \alpha 2n)^{206}Bi$	2
$(^{6}Li, \alpha pn)^{206}Pb$	1

position.

III. EXPERIMENTAL RESULTS

From the γ-excitation measurements for the bombardment of ^{206}Pb with ^{6}Li, the previously unknown 423.9-, 596.3-, 576.6-, and 724.8-keV γ rays were observed to have excitation functions that were similar to that observed for the 408.7-keV γ ray, which was known to be in ^{209}At from β decay studies of ^{209}Rn. Thus, it is expected that these γ rays originate from ^{209}At (see Fig. 1) which is produced in the $(^{6}Li, 3n)$ reaction. It was observed that, as the beam energy was increased from 29 to 34 MeV, the intensity of these γ rays, namely, the $(^{6}Li, 3n)$ cross section, became considerably larger than that for any of the other channels. In Table I, the relative intensities of the various reaction channels at 34 MeV obtained from known ground-state γ-ray transitions are listed. The $^{206}Pb(^{6}Li, 3n)^{209}At$ reaction is the strongest, although several channels involving α particles, which are principally from ^{6}Li breakup, contain considerable strength. The excitation functions for the $(^{6}Li, 3n)$ and $(^{6}Li, 2n)$ reactions were consistent with cross-section peaks expected at 40 and 26.5 MeV, respectively.[9] The $(^{6}Li, 2n)$ reaction is limited at the low end of the excitation measurements because of the Coulomb barrier.

The results of the γ-γ coincidence measurement are summarized in Table II. From these results, a level scheme for ^{209}At was constructed and is shown in Fig. 6. The most prominent feature of the decay scheme is the γ-ray cascade from the 2428-keV level to the ground state, with a branch occurring at the 725-keV level. In Fig. 2 are shown the coincidence spectra for the 423.9-, 576.6- (577), 596.3-, and 724.8-keV transitions in the cascade. From these spectra, it is not clear that the 577-, 106.1-, and 147.9-keV γ rays belong to this cascade; however, the results of the γ-γ coincidence measurement employing the intrinsic Ge detector established the 106.1- and 147.9-keV lines as members of this cascade. The assignment of the 577-keV line to this cascade will be dis-

TABLE II. Results of γ-γ coincidence and angular distribution measurements for ^{209}At.

E_γ (keV) [a]	I [b]	A_2	A_4	γ rays coincident with E_γ [c]
106.1 ± 0.2	41 [d]			
147.9 ± 0.2	49 [e]			576.6
337.6				408.7
380.3	18	−0.07 ± 0.09	−0.4 ± 0.3	408.7
386.9				(380.3), 576.6(577), (596.3), (724.8)
408.7	36			337.6, 380.3
423.9	18	−0.26 ± 0.12	−0.4 ± 0.3	576.6(577), 596.3, 724.8
530.6	8	−0.59 ± 0.15	−0.05 ± 0.05	576.6(577), 664.2
576.6 [f]	100	−0.40 ± 0.32	−0.05 ± 0.06	147.9, 423.9, 530.6, 596.3, 635.3, 664.2
577 ± 1	6			
596.3	70 [g]	+0.3 ± 0.1	−0.1 ± 0.1	106.1, 147.9, 423.9, 576.6(577), 724.8
635.3				576.6
664.2	31	−0.25 ± 0.06	−0.3 ± 0.2	530.6, 576.6
724.8	100	+0.27 ± 0.02	−0.06 ± 0.04	(386.9), 423.9, (577), 596.3

[a] All γ-ray energies, unless otherwise noted, are accurate to ± 0.5 keV.

[b] γ-ray intensities are normalized to the 724.8-keV γ-ray yield; intensities are accurate to 10% and do not include internal conversion, unless otherwise noted.

[c] Parenthesis around γ-ray energy indicates a weak coincidence.

[d] Intensity (accurate to 20%) of this transition includes internal conversion since it was obtained from the delayed component of the subsequent 596.3-keV γ ray.

[e] Intensity (accurate to 20%) of this transition includes internal conversion since it was obtained from the difference between the longer delayed components of the 576.6(577)- and the 423.9-keV photopeaks.

[f] Angular distribution data for this γ ray include the 577-keV γ-ray yield.

[g] Error in intensity is ± 30%; this error and the large error in the A_2 and A_4 coefficients are due to the neutron excitation of the 2^+ state in ^{74}Ge at 596 keV.

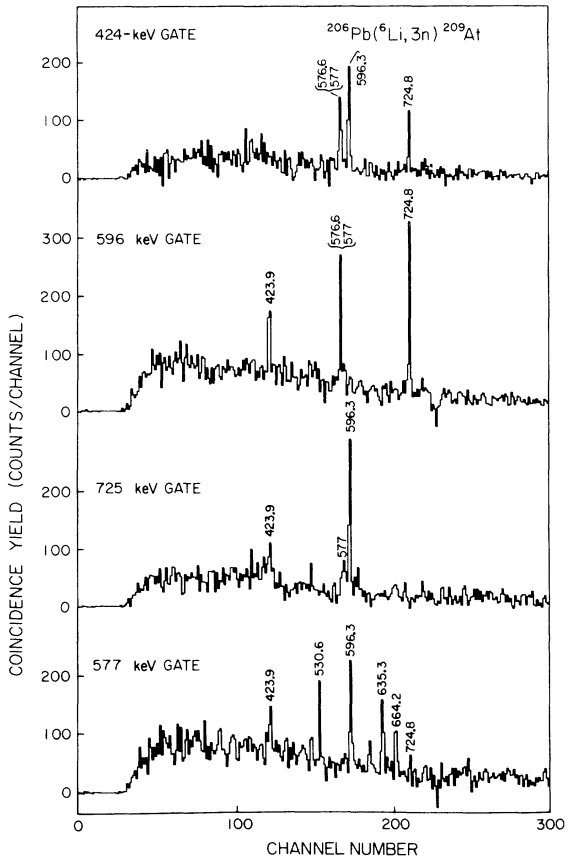

FIG. 2. γ-γ coincidence spectra from the ^{206}Pb(^{6}Li, 3n) ^{209}At reaction observed with two Ge(Li) detectors for four selected γ-ray gates. The 577-keV gate includes both the 576.6- and 577-keV γ rays.

cussed below.

All of the γ rays listed in Table II except for the 386.3-keV γ ray were assigned to the ^{209}At level scheme (see Fig. 6). Although a 386.3-keV γ ray was observed in coincidence with the 408.7-keV ground-state transition in the β decay studies of ^{209}Rn,[8] no such coincidences were observed in the present experiment. The position of the 386.3-keV γ ray could not be established on the basis of the present coincidence information shown in Table II.

The results extracted from the angular distribution measurements are also summarized in Table II. The relative γ-ray intensities are listed, as well as angular distribution A_2 and A_4 coefficients for those γ-ray transitions which could be isolated in the singles Ge(Li) spectra. An interpretation of these results in terms of γ-ray multipolarities, J^{π} assignments, and the level scheme will be given at the end of this section.

Evidence for two isomeric states in ^{209}At was found in the pulsed beam-γ timing data. It was observed in the delayed Ge(Li) spectra that the 423.9-, 596.3-, 576.6- (577), and 724.8-keV γ rays all had delayed components. Moreover, the delayed intrinsic Ge spectrum that is displayed in Fig. 3 showed that the 106.1- and 147.9-keV transitions were also delayed. The observed delayed components for these γ rays could only be explained by the existence of two isomeric states.

With the time differential measurements, the lifetimes of these isomers were found to be $T_{1/2}$ = 680(75) and 29(2) nsec for the 2428- and 1427-keV states, respectively. The half-life of the longer-lived isomer was obtained from the decay spectra of the 423.9-keV γ ray which is displayed in Fig. 4; however, a strong prompt component for the 423.9-keV γ ray remained after Compton background subtraction. This suggested that another higher lying transition was responsible for the observed lifetime. In the γ-γ coincidence experiment, a very weak 577-keV transition was observed to be connected to and above the 423.9-106.1-596.3-724.8-keV main cascade. In addition, the longer-lived delayed component of the 577-keV γ ray was larger than what could be attributed to the 576.6-keV transition. Except for the weak 577-keV line, no other delayed γ ray was found; therefore, the $T_{1/2}$ = 680(75) nsec lifetime was assigned tentatively to the 2428-keV level. The ^{209}Bi(α, 4n)^{209}At reaction, used by Bergström *et al.*[12] with 50-MeV α particles, populated the 2428-keV level with considerable strength yielding this interpretation without question.

The lifetime of the shorter lived isomer was measured by setting gates on the 596.3-, 576.6-, and 724.8-keV γ rays. The decay curve for the 596.3-keV line is shown in Fig. 4. For all three γ rays it was necessary to fit a two-lifetime function

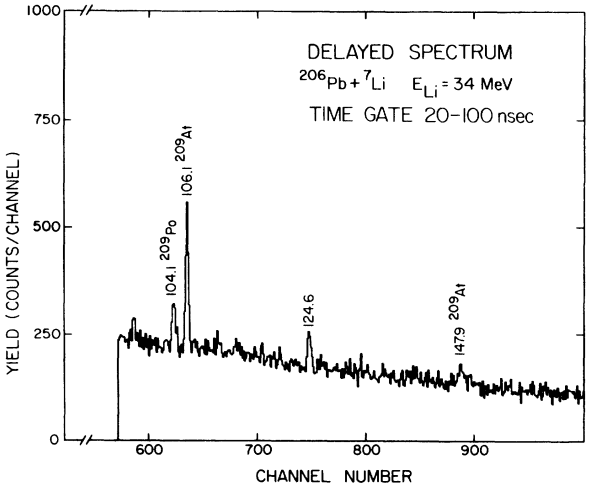

FIG. 3. Delayed γ-ray spectrum obtained with a 5-mm thick planar intrinsic Ge detector positioned at 90° to the beam.

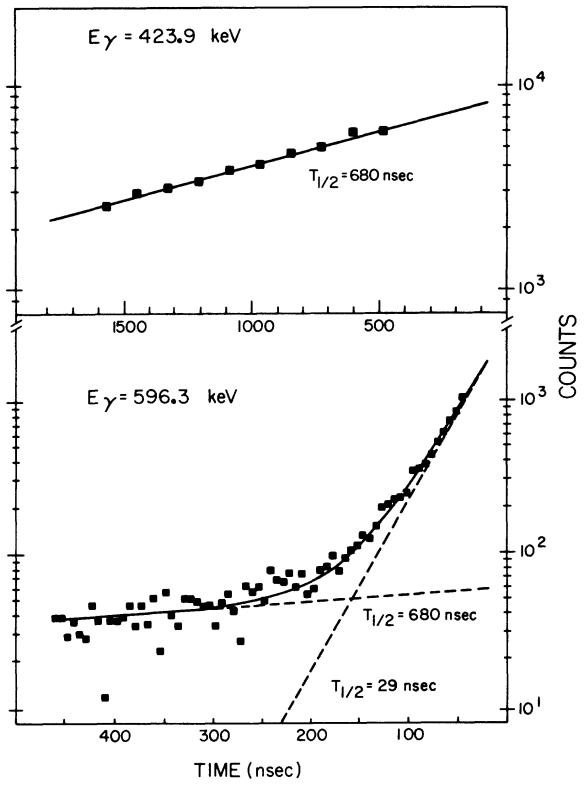

FIG. 4. Results of the time-differential lifetime measurements of the $(\frac{29}{2}^+)$ and $\frac{21}{2}^-$ states in ^{209}At obtained from the pulsed beam-γ time spectra of the 423.9- and 596.3-keV γ rays, respectively. The solid lines are least squares fits to the data. The 596.3-keV γ-ray data required a two-lifetime fit, and the dotted lines represent the lifetimes for each component.

to the data. The shorter lifetime contribution extracted from these fits was $T_{1/2} = 29(2)$ nsec, while the longer lifetime was consistent with the value obtained from the 423.9-keV transition (see Fig. 4). Since the 596.3-keV γ ray had a prompt component, the 29-nsec half-life had to originate from a higher transition. Because the 423.9-keV transition had no short lifetime component, the only possible transition left to carry the lifetime was the delayed 106.1-keV γ ray. The 29-nsec half-life was thus assigned to the 1427-keV level. Except for these two isomeric levels, the γ-ray time spectra yielded lifetime upper limits for the other levels of $T_{1/2} \leq 5$ nsec.

The uncorrected g factor of the 1427-keV $T_{1/2} = 29$ nsec state was measured to be $+0.933(19)$, and the results of this measurement are shown in Fig. 5. An attempt to determine the g factor of the $T_{1/2} = 680$ nsec state was unsuccessful, because the state was so weakly populated. Because of the weak population, the delayed feeding could be neglected for the g factor analysis of the $T_{1/2} = 29$ nsec isomer. After making corrections for Knight shift and diamagnetism with the values reported in Ref. 7, the g factor of the 1427-keV state was found to be $g = +0.95(2)$.

On the basis of experimental information obtained in the above series of in-beam γ-ray measurements, the multipolarities of the γ-ray transitions and J^π for the levels can be deduced with various degrees of confidence depending upon the nature of the experimental data. The deduced results are given in Fig. 6. The dominant decay cascade shown on the left side of Fig. 6 will be discussed first. The γ rays in this cascade decrease in intensity as the energy of the initial state increases. This feature, which is characteristic of the population of yrast levels and the subsequent $J \rightarrow J - L$ stretched γ-ray transitions, is expected in (HI, xn) fusion-evaporation reactions.[9] The less intense decay transitions, which are indicative of non-yrast levels, are shown on the right side of Fig. 6.

The similar large positive A_2 coefficients and small negative A_4 coefficients extracted from the strong 596.3- and 724.8-keV cascade transitions identify these γ rays as stretched $J \rightarrow J - 2$ $E2$ transitions; the lifetime limits obtained from these transitions eliminate the possibility of $M2$ multipolarities. Based on $J^\pi = \frac{9}{2}^-$ for the ground state of ^{209}At, these results imply J^π assignments of $\frac{13}{2}^-$ and $\frac{17}{2}^-$ for the 725- and 1321-keV levels, respectively. The large negative A_2 for the 576.6-keV transition implies a dipole component for this transition and $J = \frac{11}{2}$ for the 577-keV level. Although no angular distribution was obtained for the 147.9-keV transition, the lifetime limit for the 725-keV level suggests a dipole component for the 147.9-keV tran-

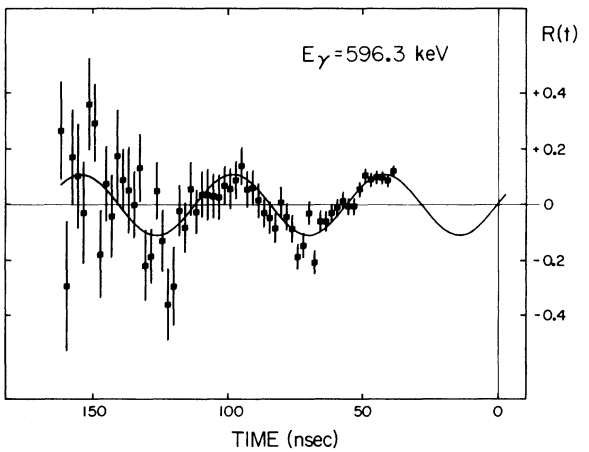

FIG. 5. Results of the perturbed angular distribution measurment of the 1427-keV $\frac{21}{2}^-$ state in ^{209}At using the 596.3-keV γ ray. An external magnetic field of 12.3 ± 0.1 kG was applied. The corrected g factor was found to be $g = 0.95 \pm 0.02$.

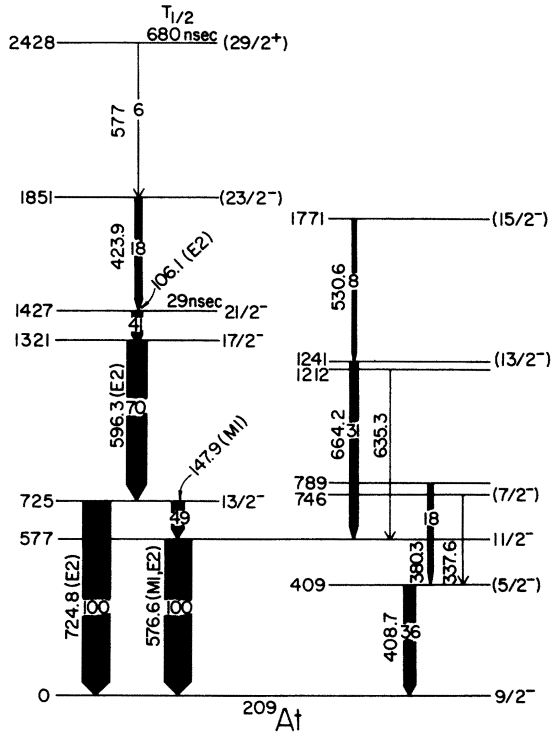

FIG. 6. The energy level scheme for ^{209}At determined from the experiment. The intensities for the 106.1- and 147.9-keV γ-ray transitions include internal conversion since they were obtained from subsequent delayed γ-ray transitions. The tentative J^{π} assignments for the 409- and 746-keV levels are taken from Ref. 8.

sition by ruling out a pure quadrupole multipolarity.

No angular distribution results were obtained for the 106.1-keV γ ray, because it is highly converted. An estimate of the internal conversion coefficient (ICC) obtained from the intensities of the delayed cascade γ rays implies that this transition is $E2$. In addition, on the basis of Weisskopf and shell-model estimates, the 29-nsec half-life is consistent with an $E2$ multipolarity.[14] Thus for yrast stretched decay, these results give an assignment of $\frac{21}{2}^-$ to the 1427-keV level.

The weak intensity of the 423.9-keV γ ray makes its angular distribution less reliable because of difficulties of isolating it from background contaminants. The negative A_2 for this γ ray suggests a dipole component, although the uncertain but possibly nonzero A_4 also suggests the mixing of a quadrupole multipolarity. An $M1/E2$ mixed 423.9-keV transition for yrast decay implies a $J^{\pi} = (\frac{23}{2}^-)$ for 1851-keV level; the bracket denotes the tentative nature of this assignment.

The weak 577-keV γ ray that deexcites the 2428-keV level is not resolved from the 576.6-keV γ ray; thus no angular distribution data were obtained.

The 680-nsec half-life measured for the 2428-keV level, however, is consistent with Weisskopf and shell-model estimates for an $E3$ transition. A tentative assignment of $J^{\pi} = (\frac{29}{2}^+)$ is thus given to the 2428-keV level.

The multipolarity and J^{π} values deduced from the above results are in agreement with those obtained in the ^{209}Bi$(\alpha, 4n)^{209}$At study at $E_{\alpha} = 50$ MeV of Bergström *et al.*[12] from ICC and γ-ray angular distribution measurements. With a larger population of the 2428-keV level by this reaction, the $\frac{29}{2}^+$ and $\frac{23}{2}^-$ assignments for the 2428- and 1851-keV levels, respectively, are stronger in their work. In the $(\alpha, 4n)$ study, the γ-ray transitions shown on the right in Fig. 6 were not observed, at least with any significant strength.

The γ-ray transitions shown on the right in Fig. 6, which were observed with generally less intensity, appear to involve non-yrast levels in ^{209}At. The angular distribution coefficients for the 664.2- and 530.6-keV γ rays were suggestive of mixed multipolarities; $M1/E2$ mixing is most probable considering the upper lifetime limits for the levels involved. Angular distributions for the other γ rays could not be extracted because of the difficulty of isolating the γ rays in the singles spectra. The 408.7-keV transition, for example, is not completely resolved from the 405.7-keV γ ray that originates in ^{207}Bi. Spin assignments made from these γ rays, if possible, are tentative; they are shown in Fig. 6 with brackets. A $J^{\pi} = \frac{5}{2}^-$ was suggested for the 409-keV level from the β studies.[8]

IV. DISCUSSION

The experimental results obtained for ^{209}At from the present ^{206}Pb(^{6}Li, $3n$) γ-ray measurements are summarized in Fig. 6 and Table II. The observed ^{209}At level scheme has a strong similarity to ^{211}At.[6] The $\frac{21}{2}^- - \frac{17}{2}^- - \frac{13}{2}^- - \frac{9}{2}^-$ sequence of yrast levels in ^{209}At have similar energies as the $(\pi h_{9/2})^3 J^-$ levels in ^{211}At except for the $\frac{13}{2}^-$ level of ^{209}At which is considerably lower. This comparison suggests that except for the $\frac{13}{2}^-$ level the neutron holes in this ^{209}At sequence are to a large extent inactive, $(\nu)^{-2}0^+$, leaving only the active $(\pi h_{9/2})^3 J^-$ nucleons as in ^{211}At. For the ^{209}At $\frac{13}{2}^-$ level at 725 keV, the $|(\pi h_{9/2})^3 \frac{9}{2}^-, (\nu)^{-2}2^+; \frac{13}{2}^-\rangle$ configuration, involving the active neutron holes, must be of more importance. This can be easily understood since the ^{206}Pb 2^+ level is at 803 keV. A similar energy reduction is observed in the 2^+ level of ^{208}Po in comparison with the $(\pi h_{9/2})^2 2^+$ level in ^{210}Po.[15]

The $(\frac{23}{2}^-)$ level at 1851 keV and the $(\frac{29}{2}^+)$ level at 2428 keV in ^{209}At are also similar in energy to the corresponding levels of ^{211}At.[6] These levels represent predominantly the $|(\pi h_{9/2})^2(\pi f_{7/2}); \frac{23}{2}^-\rangle$ and the $|(\pi h_{9/2})^2(\pi i_{13/2}); \frac{29}{2}^+\rangle$ configurations of ^{211}At which

suggests that the neutron holes in ^{209}At in these states are again inactive as $(\nu)^{-2}0^+$.

The electromagnetic properties of ^{209}At extracted from the lifetime and g-factor measurements, which are summarized in Table III, also show general similarities with the corresponding properties of ^{211}At. To study the influence of the $(\nu)^{-2}$ neutron holes in ^{209}At more carefully, the differences observed in these electromagnetic properties will be compared with theoretical values which have been calculated.

In the shell model with ^{208}Pb as a double closed shell nucleus, the ^{209}At states involve three-proton-particle plus two-neutron-hole configurations of the type $|(\pi)^3 J_p, (\nu)^{-2} J_n; J\rangle$. With wave functions made up of these configurations, it is expected that the properties of ^{209}At could be explained using the same effective interaction and effective single particle operators which are needed for other nuclei near ^{208}Pb. However, this expectation is difficult to test very accurately for ^{209}At because of the large three-particle–two-hole basis which would be needed for an exact solution. Much of the difficulty arises from the two neutron holes which are found to be complicated for ^{206}Pb and require the entire $2f$-$3p$ model space.[2,16] On the other hand, the proton components of the states in ^{209}At, for which electromagnetic properties were obtained, have simple $(\pi)^3$ configurations of $(h_{9/2})^3$ or $(h_{9/2})^2 i_{13/2}$. Assuming that the dominant configurations in these high-spin ^{209}At states are of the form $|(\pi)^3 J_p, (\nu)^{-2} J_n = 0; J\rangle$ because of the similar energies in ^{209}At and ^{211}At, then the properties of ^{209}At can be approximately calculated by using wave functions in which the amplitudes for the admixture of configurations with $J_n \neq 0$ are obtained in perturbation theory.

To test this interpretation, the electromagnetic matrix elements for ^{209}At are calculated in perturbation theory and compared with the experimental results. For this comparison, it is convenient to use the ratio of the matrix elements in ^{209}At to

TABLE III. Comparison of experimental and theoretical $B(E2)$ and g-factor results in ^{208,210}Po and ^{209,211}At.

$J_i \to J_f$	Nucleus	$B(E2)$ (e^2fm^4)	$\tilde{e}_p = \frac{e_p\,(N=124)}{e_p\,(N=126)}$	$(\pi)^n$ configuration	Experiment [a] $\delta\tilde{e}_p$	Theory $\delta\tilde{e}_p'$	Theory $\delta\tilde{e}_p''$
$6^+ \to 4^+$	^{208}Po	~469 [b]	~1.20	$(1h_{9/2})^2$	~0.20		
$6^+ \to 4^+$	^{210}Po	247 ± 33 [c]					
$8^+ \to 6^+$	^{208}Po	~106 [b]	~1.38, (1.3 ± 0.1) [d]	$(1h_{9/2})^2$	~0.38, (0.3 ± 0.1) [d]	0.38	0.43
$8^+ \to 6^+$	^{210}Po	73 ± 6 [c]					
$\frac{21}{2}^- \to \frac{17}{2}^-$	^{209}At	203 ± 17 [e]	1.24 ± 0.08	$(1h_{9/2})^3$	0.24 ± 0.08		
$\frac{21}{2}^- \to \frac{17}{2}^-$	^{211}At	131 ± 13 [c]					
J	Nucleus	g	$\tilde{g}_p = \frac{g_p\,(N=124)}{g_p\,(N=126)}$	$(\pi)^n$ configuration	$\delta\tilde{g}_p$	$\delta\tilde{g}_p'$	$\delta\tilde{g}_p''$
8^+	^{208}Po	0.913 ± 0.010 [f]	1.003 ± 0.016	$(1h_{9/2})^2$	0.003 ± 0.016	0.029	0.003
8^+	^{210}Po	0.910 ± 0.010 [f]					
$\frac{21}{2}^-$	^{209}At	0.95 ± 0.02 [e]	1.04 ± 0.03	$(1h_{9/2})^3$	0.04 ± 0.03		
$\frac{21}{2}^-$	^{211}At	0.917 ± 0.016 [g]					
$\frac{29}{2}^+$	^{209}At	1.06 ± 0.02 [h]	0.99 ± 0.03	$(1h_{9/2})^2 1i_{13/2}$	−0.01 ± 0.03	0.019	0.002
$\frac{29}{2}^+$	^{211}At	1.073 ± 0.031 [g]					

[a] $\delta\tilde{e}_p = [e_p\,(N=124)/e_p\,(N=126)] - 1$; $\delta\tilde{g}_p = [g_p(N=124)/g_p\,(N=126)] - 1$.

[b] The $B(E2)$ values for the $6^+ \to 4^+$ and $8^+ \to 6^+$ transitions in ^{208}Po are only rough estimates because of the limited lifetime information for the 6^+ state and because the transition energy from the 8^+ state is unknown, see W. Tretyl, E. Hyde, and T. Yamazaki, Nucl. Phys. A117, 481 (1968).

[c] Reference 14.

[d] The quadrupole moment ratio of the 8^+ state in ^{208}Po to the 8^+ state in ^{210}Po is 1.3 ± 0.1; see F. V. Feilitzsch, T. Faestermann, O. Häusser, K. E. Löbner, R. Lutter, H. Bohn, D. J. Donahue, R. L. Hershberger, and F. Riess, in *Proceedings of the International Conference on Hyperfine Interactions, Uppsala,* 1974, edited by E. Karlsson and R. Wäppling (Univ. of Uppsala, Uppsala, 1974), p. 142.

[e] Present experiment; the $B(E2)$ was calculated with an ICC = 6.14(± 5%), R. S. Hager and C. E. Seltzer, Nucl. Data A4, 1 (1968) and O. Dragoun, Z. Plajner and F. Schmutzler, Nucl. Data A9, 119 (1971); the results from Ref. 12 are $B(E2) = 245 \pm 15\ e^2\text{fm}^4$ ($T_{1/2} = 25 \pm 1$ nsec) and $g = 0.88 \pm 0.06$.

[f] S. Nagamiya, in *Proceedings of the International Conference on Nuclear Moments and Nuclear Structure,* edited by H. Horie and K. Sugimoto [J. Phys. Soc. Jpn. Suppl. 34, 619 (1973)].

[g] Reference 7.

[h] Reference 12.

those in ^{211}At. The electromagnetic matrix elements to be checked involve the observed $E2$ transition rates and magnetic moments. These matrix element ratios, which are denoted $\tilde{e}_p$ and $\tilde{g}_p$, are obtained from the experimental $B(E2)$ values and magnetic moments by $\tilde{e}_p \equiv \{B(E2)[J_i \to J_f, {}^{209}\mathrm{At}]\}^{1/2}/\{B(E2)[J_i \to J_f, {}^{211}\mathrm{At}]\}^{1/2}$ and $\tilde{g}_p \equiv [\mu(J, {}^{209}\mathrm{At})]/\mu(J, {}^{211}\mathrm{At})]$. The $\tilde{e}_p$ and $\tilde{g}_p$ then become the effective proton $E2$ charges and g factors in ^{209}At relative to ^{211}At. The experimental values for these ratios are given in Table III for the $E2$ transitions and magnetic moments which have been measured in both nuclei. Also in Table III, these ratios are given for ^{208}Po and ^{210}Po which, because of their respective $(\pi)^2(\nu)^{-2}$ and $(\pi)^2$ structure, should yield a similar comparison.

In the simplest first-order perturbation calculation, the zeroth-order wave function was taken to have a neutron structure of $(3p_{1/2})^{-2}J_n = 0$. Then, admixtures containing neutron structures of $(3p_{1/2}{}^{-1}3p_{3/2}{}^{-1})J_n = 1, 2$ and $(3p_{1/2}{}^{-1}2f_{5/2}{}^{-1})J_n = 2$ were considered. The energy denominators for the amplitude calculations of these admixtures were taken from the single particle energy spectrum in ^{207}Pb,[17] $\epsilon(3p_{3/2}) - \epsilon(3p_{1/2}) = 0.57$ MeV and $\epsilon(2f_{5/2}) - \epsilon(3p_{1/2}) = 0.89$ MeV. The dependence on the transition energy E_γ, which was small for the cases considered, was ignored. Calculations for $\delta\tilde{e}_p$ and $\delta\tilde{g}_p$ were then carried out using standard first-order perturbation theory.[18]

The effective proton-neutron interaction was taken as a δ function with the spin-singlet and spin-triplet strengths fixed from ^{208}Bi energy levels which have $1h_{9/2}3p_{1/2}$ configurations; $V(\vec{r}) = 524(1 + 0.22\vec{\sigma}_1 \cdot \vec{\sigma}_2)\delta(\vec{r})$ MeV fm^3. Harmonic oscillator radial wave functions were used with $\hbar\omega = 41A^{-1/3} = 6.9$ MeV. With this value of $\hbar\omega$, an effective neutron charge of about $0.8e$ is needed to reproduce the experimental transitions strengths[14] in ^{207}Pb; this value was used in the calculations. The effective neutron matrix element $\langle 3p_{3/2}||M1||3p_{1/2}\rangle$ was obtained from $B(M1)_{\mathrm{exp}}[{}^{207}\mathrm{Pb}, \frac{3}{2}^- \to \frac{1}{2}^-] = 0.41\mu_N{}^2$.[19] Finally, the effective proton $E2$ charge and g factors were taken from ^{211}At[7,14]; $e_p(h_{9/2}) = 1.5$, $g_p(h_{9/2}) = 0.92$, and $g_p(i_{13/2}) = 1.31$.

The results of the calculation are given in Table III in the form $\delta\tilde{e}_p = \tilde{e}_p - 1$ and $\delta\tilde{g}_p = \tilde{g}_p - 1$. In first-order perturbation theory, the enhancements denoted $\delta\tilde{e}_p'$ and $\delta\tilde{g}_p'$ are independent of n, J_i, and J_f for a transition (or moment) with a proton structure $(\pi j)^n J_i \to (\pi j)^n J_f$, a result which is consistent with experiment for the nuclei and transitions considered in Table III. The first-order calculation gave $\delta\tilde{e}_p' = 0.38$ for the $1h_{9/2}$ orbital which is relatively large and in good agreement with the experimental average. For the change in the proton g factors, this calculation gave $\delta\tilde{g}_p'$ values which are small for the $1h_{9/2}$ and $1i_{13/2}$ orbitals and also in agreement with experiment.

The actual wave functions of the two-neutron-hole system in ^{206}Pb are not as simple as those used in the above calculation; however, the effects of this difference can be estimated by considering the known experimental properties of the 1^+ and 2^+ states in ^{206}Pb.

In the macroscopic model,[17] $\delta\tilde{e}_p$ is proportional to the inverse energy-weighted transition strength for the 2^+ states in ^{206}Pb, $W(E2) = \sum_i\{B(E2)[2_i^+ \to 0^+]\}/[E(2_i^+)]$. Using the simple $(\nu)^{-2}$ configurations which were assumed for the first-order calculation and the appropriate energies, a first order $W(E2)'$ can easily be evaluated. Thus, assuming that the coupling constant which relates $\delta\tilde{e}_p$ and $W(E2)$ is consistent with the microscopic calculation, the value of $\delta\tilde{e}_p$ which incorporates the experimental properties of ^{206}Pb is given by $\delta e_p'' = (\delta e_p')[W(E2)_{\mathrm{exp}}/W(E2)']$.

The main contribution to $W(E2)_{\mathrm{exp}}$ comes from the first excited 0.803-MeV ^{206}Pb 2^+ state which has $B(E2)_{\mathrm{exp}}[2^+ \to 0^+] = 184\ e^2fm^4$.[19] Thus $W(E2)_{\mathrm{exp}} = 228\ e^2fm^4$/MeV, and comparing this with $W(E2)' = 203\ e^2fm^4$/MeV, the result for the effective charge is $\delta\tilde{e}_p'' = 0.43$. This represents a rather small change from $\delta\tilde{e}_p'$ and is still in agreement with experiment.

A similar procedure can be carried out to relate the g-factor ratio with the $M1$ transition strength in ^{206}Pb. In this case, $W(M1)' = 0.98\mu_N{}^2$/MeV. Only one 1^+ state at 1.70 MeV in ^{206}Pb has been observed to decay to the ground state; $B(M1)_{\mathrm{exp}} = 0.17 \pm 0.03\mu_N{}^2$,[20] which gives $W(M1)_{\mathrm{exp}} = 0.10\mu_N{}^2$/MeV. This then leads to a large reduction in the g-factor ratio, $\delta\tilde{g}_p'' = 0.10\delta\tilde{g}_p'$. Unfortunately, the experimental error for $\delta\tilde{g}_p$ is too large to distinguish between $\delta\tilde{g}_p''$ and $\delta\tilde{g}_p'$. However, with such a small value for $\delta\tilde{g}_p''$ which is due to admixtures of the $(\nu)^{-2}1^+$ states, the influence of the admixtures of the $(\nu)^{-2}2^+$ states on the g-factor ratio should also be considered. The effect of the $(\nu)^{-2}2^+$ admixture has previously been estimated to be small for the high-spin $(\pi)^2$ configurations in ^{208}Po,[21] but in the similar case of the proton $2d_{3/2}$ and $3s_{1/2}$ hole orbitals in ^{205}Tl, shell-model calculations show that the 2^+ admixture is important especially for the $2d_{3/2}$ proton state.[3]

It is interesting to compare the preceding microscopic calculation with the semimicroscopic description for ^{209}At given by Paar.[4] In the semimicroscopic picture, ^{209}At is calculated exactly assuming $(h_{9/2})^3$ for the proton configuration, a 0^+ ground state, and 2^+ quadrupole vibration for the neutron configuration. The proton-neutron interaction is taken as a cluster-vibration interaction. The results of this calculation are similar to the present microscopic calculation in that the additional proton effective charge is almost independent

of J_i and J_f. However, Paar's quantity $\delta\tilde{e}_p = 0.94$ is twice as large as the result of the present calculation and experiment. This indicates that the cluster-vibration coupling strength used by Paar has been overestimated. The amplitude for the configuration $|J_p = J - 2, J_n = 2; J\rangle$ for the $J = \frac{17}{2}$ and $\frac{21}{2}$ states in ^{209}At is about -0.33 in Paar's calculation and about -0.15 in the present calculation.

It is also interesting to compare the energy level shifts between ^{209}At and ^{211}At which again can be related to the differences in the ^{206}Pb and ^{208}Pb cores. A qualitative understanding of the energy shift can be obtained from Paar's calculation, but it is difficult to make a quantitative comparison with experiment because of the approximations which were used for the $(\pi)^3$ interaction and the energy of the ^{206}Pb 2^+ vibration. Bergström *et al.*[12] have been able to explain the energy shift for a number of high-spin states relative to the ^{206}Pb and ^{208}Pb cores by introducing an additional phenomenological P_2 force; this is the modification expected[22] for a coupling with the low-lying ^{206}Pb 2^+ vibration (particle-hole state) and is thus closely related to the effective proton charge $\delta\tilde{e}_p$. The energy level shifts have not yet been calculated in microscopic perturbation theory.

In the above comparisons for the $N = 124$ nuclei, the high-spin states are assumed to have dominant zeroth-order components $|(\pi)^n J_p, (\nu)^{-2} J_n = 0; J\rangle$. However, because of the low energy for the first 2^+ state in ^{206}Pb there are many cases where this assumption breaks down even for the yrast levels and more exact calculations should be made. Examples of this are the lowest $\frac{11}{2}^-$ and $\frac{13}{2}^-$ states in ^{209}At ($n = 3$) which should have dominant components with $J_n = 2$. Similar states are found in ^{207}Bi ($n = 1$).[23] Another case is the lowest $\frac{5}{2}^+$ state in ^{205}Tl ($n = -1$) which has been shown in a shell-model calculation by Zamick *et al.*[3] to have a dominant $(\nu)^{-2} J_n = 2$ neutron-hole structure.

---

†Supported in part by the National Science Foundation.

*Max Kade Fellow, University of Erlangen, Germany.
‡On leave from Tata Institute of Fundamental Research, Bombay, India.
§Present address: Michigan State University, East Lansing, Michigan.
¶Present address: Brooklyn College, City University of New York, Brooklyn, New York.

[1]J. B. McGrory and T. T. S. Kuo, Nucl. Phys. A247, 283 (1975).
[2]G. H. Herling and T. T. S. Kuo, Nucl. Phys. A181, 113 (1972).
[3]L. Zamick, V. Klemt, and J. Speth, Nucl. Phys. A245, 365 (1975).
[4]V. Paar, Phys. Rev. C 11, 1432 (1975).
[5]See for example, A. de-Shalit, Phys. Rev. 122, 1530 (1961); A. Covello and G. Sartoris, Nucl. Phys. A93, 481 (1967); and Ref. 3.
[6]I. Bergström, B. Fant, C. J. Herrlander, K. Wikstrom, and J. Blomqvist, Phys. Scr. 1, 243 (1970); K. H. Maier, J. R. Leigh, F. Puhlhofer, and R. M. Diamond, Phys. Lett. 35B, 401 (1971).
[7]H. Ingwersen, W. Klinger, G. Schatz, and W. Witthuhn, Phys. Rev. C 11, 243 (1975); C. V. K. Baba, D. B. Fossan, W. Hering, D. Proetel, T. Faestermann, F. Feilitzsch, and K. E. G. Löbner, Bull. Am. Phys. Soc. 17, 927 (1972).
[8]B. Jonson, M. Alpsten, A. Appelqvist, B. Bengtsson, and K. A. Johansson, Phys. Scr. 8, 142 (1973); Ts. Vylov, N. A. Golovkov, K. Ya. Gromov, I. I. Gromova, A. Kolachkovski, M. Ya. Kuznetsova, Yu. V. Norseev, and V. G. Chumin, Isv. Akad. Nauk SSSR Ser. Fiz. 38, 701 (1974) [Bull. Acad. Sci. USSR Phys. Ser. 38, 31 (1974)].
[9]J. O. Newton, in *Nuclear Spectroscopy and Reactions, Part C*, edited by J. Cerny (Academic, New York, 1974), p. 185.
[10]See for example, B. A. Brown, P. M. S. Lesser, and D. B. Fossan, Phys. Rev. C 13, 1900 (1976).
[11]G. Schatz, T. P. Sjoreen, S. K. Bhattacherjee, B. A. Brown, D. B. Fossan, and P. M. S. Lesser, Bull. Am. Phys. Soc. 19, 598 (1974); T. P. Sjoreen, G. Schatz, S. K. Bhattacherjee, B. A. Brown, D. B. Fossan, and P. M. S. Lesser, *ibid.* 19, 1020 (1974).
[12]I. Bergström, private communication; I. Bergström, C. J. Herrlander, Th. Lindbald, V. Rahkonen, K. -G. Rensfelt, and K. Westerberg, Z. Phys. A273, 291 (1975).
[13]E. Recknagel, in *Nuclear Spectroscopy and Reactions, Part C* (see Ref. 9), p. 93.
[14]G. Astner, I. Bergström, J. Blomqvist, B. Fant, and K. Wikstrom, Nucl. Phys. A182, 219 (1972).
[15]K. Wikstrom, I. Bergström, J. Blomqvist, and C. J. Herrlander, Phys. Scr. 10, 292 (1974).
[16]W. W. True and K. W. Ford, Phys. Rev. 109, 1675 (1958); W. W. True, *ibid.* 168, 1388 (1968).
[17]A. Bohr and B. R. Mottelson, *Nuclear Structure* (Benjamin, New York, 1969), Vols. I and II.
[18]A. E. L. Dieperink and P. J. Brussaard, Nucl. Phys. A129, 33 (1969); S. Yoshida and L. Zamick, Annu. Rev. Nucl. Sci. 22, 121 (1972).
[19]O. Häusser, F. C. Khanna, and D. Ward, Nucl. Phys. A194, 113 (1972).
[20]F. R. Metzger, Ann. Phys. (New York) 66, 697 (1971).
[21]S. Nagamiya, Y. Yamazaki, O. Hashimoto, T. Nomura, K. Nakai, and T. Yamazaki, Nucl. Phys. A211, 381 (1973).
[22]A. Molinari, M. B. Johnson, H. A. Bethe, and W. M. Alberico, Nucl. Phys. A239, 45 (1975).
[23]M. R. Schmorak and R. L. Auble, Nucl. Data B5, 207 (1971).